Freeze Casting for Near-Net-Shaping of Dense Zirconium Diboride Ceramics

Silvia Leo,[1,3] Laura Jukes, [1,3] Samuel Pinches, [1,3] Carolina Tallon, [1,2,3]

George V. Franks[1,3]

[1]Department of Chemical Engineering, The University of Melbourne, Vic. 3010, Australia

[2]Department of Materials Science and Engineering, Virginia Polytechnic Institute and State University, Blacksburg, Virginia 24061, USA

[3]Defence Materials Technology Centre, Hawthorn, Vic 3122, Australia

Abstract

Zirconium diboride (ZrB_2) was formed into dense complex shapes using freeze casting as a near-net-shaping technique. Aqueous-based formulations were compared to non-aqueous (cyclohexane) based formulations in terms of rheological behaviour, particle packing in the green body, sintered density, macroscale porosity and cracking. The influence of particle solids concentration and freezing rate was investigated. The aqueous formulations were found to be deficient in that they produced macroscale porosity that could not be eliminated during sintering resulting in low density and large pores in the final shaped objects. The non-aqueous-based system was able to produce complex shaped objects with significantly reduced macroscale porosity. The higher concentration of solids in the non-aqueous-based formulations was primarily responsible for the reduced macroscale porosity and enabled higher sintered densities (up to 90 to 91.5% of theoretical density for fast freezing). The microstructure of the

ZrB_2 formed at fast freezing rates and high solids content typically had isolated pores in the order of 5 to 10 microns in size, mainly found along grain boundaries (grain sizes between 20 and 50 microns). Although this rapid freezing produced denser components, it tended to produce objects with internal cracks. When slower freezing rates were used, intricate complex shaped objects could be produced without cracks but their density was only between 65 and 80% of theoretical density.

KEYWORDS, freeze casting, shape forming, zirconium diboride, colloidal processing

1 INTRODUCTION

Freeze casting is a method to produce complex shaped ceramic green bodies via freezing a suspension in a complex shaped mold.[1-2] The ceramic suspension may be either poured or injected into either a pre-chilled mold or a mold at room temperature before freezing. Freeze drying is used to remove the solvent by sublimation. Most investigations on freeze casting focus on ice templating to produce porous bodies.[3-13] In those investigations the aim is to produce a macroporous green body where the solvent crystals (ice in the case of water) act as pore formers. This research has provided deep understanding about the role of freezing rate and solids concentration of the suspension on controlling microstructure of macroporous ceramics. Specifically, increased amount of porosity is produced using lower solids concentration suspensions for a given freezing rate,[3,14] and, for a given solid concentration, smaller pores generally result from increased freezing front velocity.[15]

Freeze casting has also been applied to produce dense complex shaped ceramics because of three potential advantages when compared to other near-net-shaping techniques. Firstly, there is potential of a very quick turnaround of the mold during

production, since the consolidation of the suspension via freezing in the mold happens very rapidly. For example, popsicles can be produced at a rate of over 4000 units per hour[16]; similar rates may be possible in production of ceramics. Potentially, freeze casting can produce parts at a much higher rate (per mold) than slip casting or gelcasting making freeze casting potentially more economically attractive. Secondly, the sublimative drying has the potential to reduce drying cracks by avoiding the drying stresses that result from capillary consolidation pressures that develop when a liquid is removed from a powder compact by evaporation. There is no meniscus when frozen solvent is removed from the powder body by sublimation so no capillary pressure can exist that would cause drying shrinkage and potentially differential shrinkage leading to drying cracking. Thirdly, complex shaped bodies with variable thickness cross sections in one part can be produced which cannot be achieved using slip casting. Whereas slip casting will result in variable green density throughout thick section parts, freeze casting has the potential to produce homogeneous green bodies. Freeze casting can replicate fine features sometimes difficult to produce with slip casting.

Freeze casting for dense ceramic objects has been conducted in industry for some time for the production of advanced ceramics components, although little information is available in the scientific literature. One of the first instances was the freezing of a slip cast body in order to strengthen it for unmolding.[17] Cryoprotectants were added later to avoid formation of large ice crystals that would result in large pores in the final ceramic object.[18] Some of the best industrial work on freeze casting of dense ceramics was conducted at Ceramic Process Systems Inc. in the late 1980's and early 1990s.[19-22] These researchers pioneered the use of non-aqueous solvents to avoid issues related to expansion of ice during freezing and large ice crystal formation.[21]

Freeze casting of dense ceramics began to be investigated by academics in the early 2000s.[14,23-28] Freeze casting was demonstrated to be suitable for the near-net-shape forming of complex-shaped ceramics to yield dense ceramic parts which replicate fine details of the mold. The majority of the work was conducted on oxide ceramics[14,23,24,26,27] although some work was done on AlN[25] and Si_3N_4 or SiAlONs.[20-22,28] As discussed later, these materials are relatively easy to densify. We are interested to build on this foundation work in producing dense ceramics[19-28] to develop formulations and processing techniques for "difficult-to-densify" ceramics, such as ZrB_2.

Our recently published investigation of the influence of formulation on suspension rheology compared aqueous and non-aqueous suspensions of ZrB_2, in order to used colloidal processing approaches for difficult-to-densify ceramics.[29] We showed that ZrB_2 particles are difficult to disperse in aqueous suspensions since they have the tendency to form aggregates. However, the use of a non-aqueous formulation based on cyclohexane led to the preparation of more stable and concentrated suspensions that led to high particle packing green bodies. Similar non-aqueous suspension formulations to those used in the slip casting and densification investigations[29-30] were used in this work. Cyclohexane is a suitable solvent for freeze casting since its freezing temperature (6.5^{o}C) is easily accessible as well as its low viscosity (0.89 mPa.s at 25^{o}C), high vapour pressure (97.8 mm Hg at 25^{o}C) and low toxicity.[31-33.] Furthermore, the use of the non-aqueous system avoids the issues with the volume expansion and large ice crystal formation often associated with the aqueous system.[20-22] It is recommended that the solvent used for freeze casting should have a volume change upon freezing no more

than +/- 10%.[20-21] The volume change reported for cyclohexane upon solidification is between 5.2 and 7.8% shrinkage.[34, 35]

In freeze casting, the particles can become segregated (pushed) in front of the freezing front if the freezing front velocity is slow.[15] Large ice crystals that are free of particles are formed during the freezing stage. These will be converted into large pores or channels after freeze drying and sintering. Such microstructure is the aim when ice templating is used to produce porous materials,[1, 3] but it is undesirable for high strength, dense advanced ceramic component fabrication as is the aim of the present work. Increasing the concentration of solids in the suspension reduces the tendency of segregation of particles in front of the growing ice crystals. Instead, the particles become entrapped in the growing crystal if the particle volume fraction is high enough.[15] Since the aim of the present work is to produce dense complex shaped ZrB_2 ceramics, we have increased the particle concentration to the maximum possible without increasing the viscosity beyond the point where it can be poured. In addition fast freezing will be investigated as a strategy to avoid pushing the particles in front of the solidifying solvent crystals.

The aim of the present paper is to provide proof of concept that freeze casting can be applied to a difficult-to-densify ceramics, such as ZrB_2 to produce reasonably dense complex shaped ceramic objects. The freezing speed (set by the external freezing temperature) and solid content of the slurry are two important parameters affecting the microstructure of green freeze cast bodies, and as such, the details of their initial optimisation are described in this paper. Their influence on the green and sintered microstructure, macrostructure and cracking are investigated comparing aqueous and

non-aqueous formulations. The rheological behaviour of slurries used in this work is also investigated to ensure the ease of injection.

2 EXPERIMENTAL

2.1 Materials

Zirconium diboride (ZrB_2; grade B, H.C. Starck, (Germany)) was used as the raw material. Characteristics of the powder published previously[29] are summarized as: D_{50} of 2.3 μm; 1.1 wt % oxygen. Suspensions were prepared in both deionized (DI) water (milliQ) and cyclohexane (Sigma Aldrich (Australia)). The commercially available dispersant used for the aqueous formulation is Dolapix CE 64 (Zschimmer and Schwarz, Germany). Dolapix CE 64 has been reported as an ethanolaminic salt of citric acid by Rao and Dakskobler.[36-37] The commercial dispersant used for the non-aqueous formulation is Hypermer A70 (Croda, UK). This dispersant has been previously characterized as a block copolymer with hydroxyl and amine functional groups. [38]

2.2 Preparation and characterization of ZrB_2 suspensions

The aqueous and non-aqueous formulations used in this work were prepared based on our previous research optimizing solid concentration, solvent type, dispersant type and amount.[29] From our previous work, we knew that the non-aqueous formulations produce much more homogeneous and concentrated suspensions than their aqueous counterparts do. For this reason, the number of samples and conditions studied with aqueous formulations was smaller (smaller batches with sonication to break

agglomerates) than the number of samples studied with the non-aqueous formulation (larger batches using ball milling to break agglomerates).

2.2.1 Aqueous suspensions

Aqueous suspensions (100 mL) were prepared by dispersing 45 vol % ZrB_2 powder into deionized water containing 1 wt% of dispersant (Dolapix CE 64) with respect to the powder weight. The pH of the suspension was 9.9. The suspensions were sonicated for three minutes to disperse the powders and break any agglomerates and then, rolled overnight prior to rheological measurements or freeze casting. No cryoprotectant was added to the suspension.

2.2.2 Non-aqueous suspensions

Non-aqueous ZrB_2 suspensions (100 mL) were prepared in a polyurethane-lined ball mill (Paul O. Abbe, Bensenville, IL; ID = 10.5 cm, height = 11 cm) (at a rotational speed of 250 rpm for 7 hours) with 100 mL of WC media (diameters of 0.25, 0.375, 0.5, and 0.625 inch (25 mL of each size) Glen Mills, Inc., Clifton, NJ). The powder, solvent (cyclohexane) and dispersant were added to the polyurethane-lined milling container together with the WC milling media. After ball-milling, the suspensions were kept on a roller overnight prior to casting or rheological measurement. 1 wt% Hypermer A70 with respect to powder weight was used. 50, 52 and 54 vol% solids suspensions were prepared. Although procedures were in place to minimize evaporation of cyclohexane, the suspensions were found to have increased their solids concentration to 54, 56 and 59 vol % solids just prior to freeze casting.

2.2.3 Rheological measurements

Viscosity data as a function of shear rate were collected using an AR-G2 rheometer (TA Instruments, USA) with concentric cylinders geometry (cup ID = 30 mm, rotor OD = 28 mm, rotor length = 42 mm). For each measurement, 20 mL of suspension were transferred into the cup, the rotor was lowered until its whole surface was immersed in the suspension and the measurement was started within 15 seconds after pouring into the cup. The lid specially designed to avoid contact with the rotor shaft was used to prevent evaporation of the suspension during measurement. All suspensions were subjected to increasing shear rates from 0.1 to 1000 s^{-1} in 10 minutes at a constant temperature of 25^{o} C. Although only one set of data for each condition is shown in the figures to avoid cluttering, several measurements were repeated with good reproducibility between the measurements.

2.3 Freeze casting and freeze drying

2.3.1 Molds

Two different anodised aluminium molds were used for freeze casting.

a) Closed cavity molds. The majority of the samples produced had cylindrical shape, using the closed cavity mold shown in Figure 1(a and b). The cylindrical section of the interior of the mold was 16.6 mm in height and 20 mm in diameter. A syringe containing the suspension, described in section 2.3.2. is used to fill the pre chilled mold from the bottom (plug flow) to create a frozen body (Figure 1 c and d). To demonstrate

the ability to form complex-shaped objects, another closed cavity mold was used to produce rotor-shaped objects.

b) Open cavity molds. A second aluminium mold with cylindrical cavities (similar to an ice cube tray) shown in Figure 1e was filled at ambient temperature then placed in the freezer to slowly freeze. Various chocolate, candy and novelty ice cube molds were used as well to demonstrate the shaping capability. The majority of these were made of silicone rubber and were filled at ambient room temperature and placed in the freezer for solidification.

2.3.2 Mold filling and freezing

a) Fast freezing in pre-chilled closed-cavity-molds. The closed cavity molds were pre-chilled in the freezer (at temperatures ranging from 0 to -80^{o}C) prior to freeze casting. To make cylinders, the suspension was injected into the pre-chilled closed cavity mold through a teflon injection port (kept at room temperature until just before injection) using a 60 ml catheter tip syringe (Terumo, Sydney, NSW) as shown in Figure 1 (c and d). Approximately 10 mL of suspension was drawn into the syringe and injected into the mold upside down, as shown in Figure 1 (c and d). It took approximately 1-3 seconds to inject the suspension into the mold, depending on the solid content of the slurry (i.e. it took ~1 second to inject a suspension of 54 vol% ZrB_2 in cyclohexane, while it took about 3 seconds to inject a higher viscosity suspension containing 59 vol% ZrB_2 in cyclohexane into the mold). Air was allowed to escape through small holes in the bottom part of the mold (facing upward during injection). The injected suspension was held under pressure for 10 seconds before flipping the

mold over and slowly releasing the pressure. The filled mold was then kept in the freezer set at the specified temperature for one hour. The freezing rate was estimated by measuring the temperature in the center of the cylindrical mold with a thermocouple (Type-K) as a function of time after filling the mold with a 55 vol% ZrB_2 in cyclohexane suspension. The rate of freezing was taken as the time it took the center of the suspension to decrease from 10°C to 7°C (just above the freezing point of cyclohexane) divided by that temperature difference (3°C).

b) Slow freezing in open-cavity-molds filled at ambient temperature. The aluminium mold with open cylindrical cavities as well as the novelty rubber molds were filled at ambient temperature then placed in the freezer pre-set to temperature between -20 and -80°C.

2.3.3 Freeze drying

The frozen sample was unmolded and placed in a tray pre-chilled to the same temperature used for freeze casting. The tray was placed in the freeze dryer (LyoQuest, Telstar, Spain) for freeze drying at room temperature and ~1 mbar vacuum for 24 hours with the condenser temperature at -85°C. The freeze dried samples have a cylindrical geometry with a cone shape at one end, as shown in Figure 1f. The cylindrical part of the sample is 16.6 mm in height and 20 mm in diameter. The conical part within the sprue section was about 8 mm in height. These cylindrical samples were used to investigate the influence of process parameters, such as suspension solid concentration and freezing temperature on the properties (density and microstructure) of the sintered samples.

2.3.4 Sintering and characterization

All samples were pressureless sintered in a graphite vacuum furnace (Red Devil, R. D. WEBB, Natick, MA, USA). Specimens were placed in a graphite crucible and heated at 5°C/min from room temperature to 400° C in a mild vacuum (~1 x 10^{-2} mbar), followed by 2 hours isothermal hold at this temperature to ensure the complete removal of organics. The samples were then heated at 5°C/min to the maximum temperature of 2100°C and soaked for 60 minutes. Above 1800°C, the furnace was backfilled with argon to protect the furnace elements. The samples were cooled down at 5°C/min from the maximum temperature to 1500°C and at 10°C/min from 1500°C back to room temperature.

The bulk density of green and sintered specimens was determined using Archimedes' principle. To prevent liquid ingress into the green bodies they were coated in wax as described previously.[39] The sintered samples were not coated with wax. The density values reported for green and sintered samples correspond to the average value of between 2 to 4 samples. The sintered specimens were cut in cross-section (Accutom-50, Struers, Copenhagen, Denmark), mounted in epoxy resin (Struers), and polished with SiC papers and diamond suspensions down to 6 μm using the TegraPol-21/TegraForce-5/TegraDoser-5 Polishing System (Struers). The microstructures of the central region of the specimens were characterized using a FEI Quanta FEG 200 scanning electron microscope (FEI, Hillsboro, OR), equipped with an INCA X-act 10mm energy dispersive X-ray spectrometer (Oxford Instruments, UK). Because it is difficult to section and polish green bodies, the green microstructure was observed by examining sectioned and polished sections of bisque fired specimens. The bisque firing was conducted in the Red Devil furnace described above at 1600°C for 30 minutes in argon atmosphere. Sectioning and polishing was the same as for the fully sintered

samples. Images of the central portion of the bisque fired samples were taken with a Zeiss NanoFab He ion microscope.

3 RESULTS

3.1 Suspension rheology

Figure 2 shows the viscosity versus shear rate for the 45 vol% solid ZrB_2 aqueous suspension when 1 wt% (by weight of solid) Dolapix CE 64 was used as dispersant. 45 vol% solids was found to be the maximum solids content that could be incorporated into suspension without producing a suspension with viscosity greater than 1 Pa.s at a shear rate of 30 s^{-1}. This value is considered the maximum viscosity that results in easy pourability and good mold filling. Also shown in Figure 2, significantly higher solids contents could be achieved in cyclohexane compared to water. The viscosity versus shear rate profiles of ZrB_2 suspensions containing 54-59 vol% solids in cyclohexane dispersed with 1wt% (by weight of solids) Hypermer A70 were found to be less viscous than the aqueous formulation at only 45 vol% solids. All the suspensions in cyclohexane with solid concentration of 59 vol% or below maintained low viscosities (below 1 Pa.s at a shear rate of 30 s^{-1}) suitable for pouring and injection. This indicates that the ZrB_2 suspensions remained stable and well-dispersed with solid concentration up to 59 vol%. Suspensions prepared at 61 vol% solids were too viscous to process. The reason for the better dispersion in cyclohexane compared to water is the longer range of the steric repulsion of the Hypermer in cyclohexane and the higher Hamaker constant of ZrB_2 in water as explained previously.[29]

3.2 Density, macrostructure and microstructure

3.2.1 Density

Freezing is the critical stage in freeze casting that determines the porosity and overall microstructure of the green cast.[3] The shape and size of the pores are strongly affected by the rate of ice crystal growth determined by the freezing temperature and thermal mass of the suspension and the mold.[3,40] As discussed previously,[30] when preparing dense components, uniformly distributed, fine pores in the green microstructure are desirable to yield high sintered densities. The effect of freezing rate in the current work was controlled by varying the temperature of the mold during filling (either pre-chilled or ambient room temperature) and the temperature of the freezer where the mold is placed. Figure 3 shows the temperature at the centre of the cylinder mold cavity as a function of time for both injection into pre-chilled molds and when the molds were filled at ambient temperature and placed into the freezer, for several freezing temperatures. The freezing rate was estimated as the gradient of these curves between 10 and 7ºC shown in Table S1 in the supporting information. These measurements showed that for our set-up, the range of freezing rates varied from about 0.0055 ºC/s (when the mold is filled at ambient temperature and placed in freezer set to 0ºC) to 2.5 ºC/s (when injected into a mold pre-chilled to -80ºC).

Shrinkage during freezing and freeze-drying was negligible. The green densities of the specimens were not affected by the freezing temperature for a given solid content suspension, and were found to be similar to the solid contents of the suspensions used for freeze casting. For example, an average green density of 54.2 ± 0.3 %TD was

obtained from four samples frozen at different temperatures using suspensions containing 54 vol% solid.

The sintered densities of the ZrB_2 cylinders freeze cast from 45 vol% solids aqueous suspensions were between 64 and 70% of theoretical density (TD) as shown in Table S2 in the supporting information. Sintered densities of ZrB_2 compacts freeze cast at different freezing rates using cyclohexane suspensions containing 54-59 vol% solid were between 65 and 94% theoretical density (TD) and are plotted in Figure 4 and presented in Table S3 in the supporting information.

For all non-aqueous suspensions (54-59 vol% solid), it can be seen that the sintered density generally increased with decreasing freezing temperature for both pre-chilled and ambient filled molds. This trend was most obvious in the pre-chilled molds when suspensions of lower solid concentration (54 vol% solid in suspensions) were employed for freeze casting. As shown in Figure 4, a significant improvement in the sintered density was observed when using pre-chilled molds by decreasing the freezing temperature from 0 to -40^{o}C; a further decrease of freezing temperature (from -40 to -80^{o}C) did not affect the sintered density significantly. When the slower freezing was conducted in the ambient filled molds the sintered densities were lower than those found when the mold was chilled before freezing. The trend in increasing density with decreasing freezing temperature is also found in the ambient filled molds. Figure 5 shows the trend in increasing density with increasing freezing rate for the samples cast from 59 v% solids cyclohexane suspensions. A linear trend is observed when density is plotted against the log of freezing rate, but the reason for this dependence is not known.

3.2.2 Macrostructure

Figure 6 shows low magnification SEM images of the sintered ZrB_2 produced by freeze casting 45 vol% solids aqueous suspensions. Large lamellar and dendritic pores were observed for the slowest freezing with slightly finer features observed for faster freezing consistent with previous work.[3-13] The large pores which were produced when ZrB_2 particles were rejected in front of the growing ice crystals were too large to be eliminated during sintering as discussed in detail later. The pores are between 20 to 50 microns wide by several hundred microns long for the faster freezing, (Figure 6a) and 100 or more microns wide and up to nearly 1 mm long for the slower freezing, (Figure 6c). The low density and large pores make the aqueous freeze casting system unsuitable for producing dense, high strength complex shaped ZrB_2 components. The addition of glycerol as cryoprotectant was investigated but found to reduce the size of the macropores only minimally compared to the cyclohexane formulation discussed next.

Figure 7a is a schematic illustration of how the ceramic particles in a dense suspension can be pushed in front of growing solvent crystals during slow freezing.[3,15] In order to have an idea of the green microstructure, images of samples bisque fired at 1600^{o}C for 30 minutes in argon are presented in Figure 7b-e since it is very difficult to section and polish green samples. No measurable shrinkage was found to occur during bisque firing and the density of the samples only increased from 54.2 ± 0.3% TD to 57.3 ± 0.8 % TD. As shown in the Figure 7c and e only necking between particles occurred. Figure 7b indicates that the freezing front velocity of 54 vol% solids cyclohexane suspensions frozen in a -40^{o}C prechilled mold was sufficiently high to engulf the particles in the growing solvent crystals. No pores with dimension greater than about 10 μm are observed. On the other hand, when the same suspension was poured into an

ambient temperature mold and placed in a freezer at -20°C the freezing front velocity was slow enough to allow some particles to be pushed in front of the growing ice crystals. After freeze drying the voids created by the ice crystals remained as pores with dimensions from about 20 μm in width and about 100 or more μm in length as shown in Figures 7d and e.

The low magnification SEM images of the macrostructure of sintered cylinders freeze cast from 54 vol% solids cyclohexane suspensions presented in Figure 8 show that no large scale pore structure persists after sintering. In the case of the pre-chilled closed-cavity mold shown in Figure 8a, the density is 90 % of theoretical and the pores are mainly isolated pores on order of about 5 to 20 microns in size. Such microstructure persists over 1 mm^2 area in 2D (shown in Figure 8a) and perhaps on similar scale in 3D. When the freezing rate is slower such as in the material produced by filling the closed-cavity mold at ambient temperature and freezing in a freezer set at -20°C, the cyclohexane formulation results in a microstructure featuring pores with dendritic appearance and length 100 to 200 microns with width up to 10 to 30 microns (as shown in Figure 8b). Such features are far less frequent (on a per volume basis) and less severe (smaller in size) that the large pores observed in the samples produced with aqueous formulation (Figure 6).

3.2.3 Microstructure

Figure 9 shows the difference in microstructure of sintered ZrB_2 samples freeze cast at 0 and -40°C using cyclohexane suspensions containing 54 and 59 vol% solid. The samples produced from 54 vol% suspensions, frozen at lower temperature (-40°C)

(Figure 9d-f) were found to contain more dense areas and finer pores compared to specimens frozen at 0°C (Figure 9a-c) that possessed fewer but larger pores. Considering that the samples freeze cast from 54 vol% solid suspensions at 0 and -40°C possessed similar green densities (~54 %TD), the slower frozen samples (at 0°C) did not densify as much as those of -40°C (Figure 9a-f) because of the large pores in the green bodies (due to the large ice crystals devoid of particles similar to those shown in Figure 7). Hence, it is the difference in green microstructure (pore sizes) that influences the densification behavior, not just green density.

The sintered density of freeze cast ZrB_2 depends on the suspension solid content as seen in Table S3 and Figure 4. The sintered density increased with increasing solid content in the suspension and is most pronounced at slower freezing rates. For samples frozen in molds pre-chilled to 0°C, the sintered density increased from 76.2 to 86.4 %TD for ZrB_2 as the solid concentration in the suspension was increased from 54 to 59 vol%. Given the higher green densities, green casts from 59 vol% solid suspensions are expected to contain fewer and smaller pores compared to the specimens freeze cast at the same temperature using 54 vol% solid suspensions. Both higher green density (less porosity) and smaller pore sizes contribute to the densification of these materials, allowing higher sintered densities to be reached.

The microstructures of sintered ZrB_2 freeze cast in pre-chilled closed-cavity molds at 0°C using slurries with solid content of 54 and 59 vol% are presented in Figure 9 (a-c) and (g-j) respectively. It can be seen in this figure that the specimens from 59 vol% solid suspensions correspond to denser sintered microstructures and finer pore sizes. The formation of large pores that tend to occur during slow freezing (such as in a pre-chilled closed-cavity mold at 0°C), could be minimised by increasing the solid

concentration in the suspension from 54 to 59 vol%. The microstructure of the ZrB_2 produced by rapidly freezing suspensions of high concentration, (Figure 9d-j) consist primarily of isolated pores on order of 5 to 10 microns in size mainly on the grain boundaries of grains on order of 20 to 50 microns in size.

3.3 Cracking

Based on the information provided about densities, macrostructure and microstructures provided in the previous section, one may think freeze casting with cyclohexane formulations looks like a good method to produce complex shaped ZrB_2 objects. Now we present results on cracking in the freeze cast cylinders that causes one to question the viability of freeze casting and presents new avenues for research to eliminate such defects.

Upon cutting the sintered cylindrical samples (about 17 mm in diameter and 14 mm in height) in half, most of the samples were found to have internal cracks. Photos of the typical cracks observed in the sintered ZrB_2 compacts from samples produced in pre-chilled closed-cavity molds as a function of solid volume fraction in suspension and freezing temperature are presented in Figure 10. Four types of cracking situations were observed and subjectively categorized as: *no cracks, minor, moderate* and *severe cracks*. The internal cracks found in the sintered compacts were either formed or "opened up" during the sintering process, although we cannot be certain there were no fine cracks in the dried green bodies. As seen in Figure 10, the degree of cracking worsened with decreasing freezing temperature, although the sintered densities were higher at lower freezing temperatures (see Table S3 and Figure 4). Similarly, both the sintered density and the degree of cracking increased with increasing solid content in

the slurries (see Table S3 and Figure 4). However, the freezing temperature seems to play a more important role in the degree of cracking compared to the suspension solid content. Several mechanisms that could lead to cracking will be discussed in section 4.3. There seems to be a trade off in terms of, either densification with cracking, or no cracking but low density. Neither combination is particularly satisfactory.

3.4 Complex shape forming of ZrB_2

The objects shown in Figure 11 demonstrate the capability of the freeze casting technique to produce complex-shaped ZrB_2 components, which cannot be formed by dry pressing and are difficult to obtain using slip casting. The features and sharp edges of the novelty shapes (Figure 11a), rotor (Figure 11b and c) and interlocking tiles (Figure 11d and e) were well-replicated with good dimensional accuracy, and no sign of distortion was observed in the sintered bodies. Molding conditions to produce slow freezing were used to avoid formation of large cracks but resulted in less than fully dense components as explained previously.

4 DISCUSSION

4.1 Formation and removal of large pores

During the freezing of the slurry, interactions between the suspended particles and the solvent solid/liquid interface may result in particles either being engulfed in or pushed ahead of the advancing freezing front.[3,4,41] The transition from pushing to trapping of particles by the freezing front with increasing freezing rate has been well reported in the literature.[3,7,10,42-47] If the freezing rate is slow, particles are more likely to

be pushed ahead of the freezing front as shown in Figure 7a and thus, slow freezing is often associated with large pores in the green freeze cast bodies.[10,42-44] Faster freezing (using lower freezing temperatures) tends to result in a more uniform particle distribution and finer pore sizes.[10,48]

If the particles are rejected and pushed ahead of the freezing front, the particle concentration ahead of the freezing front gradually increases until a phenomenon referred to as "breakthrough" [15,49,50] occurs, in which piled-up particles cease to be pushed along by the solid front. At this point, the solid/liquid interface pushes into the concentrated particle region and into the inter-particle spaces, trapping the particles in between the frozen medium. The pushing of particles ceases as the volume fraction of particles ahead of the solid/liquid interface reaches a certain packing density known as the breakthrough volume fraction ($\emptyset = \emptyset_b$). Once the solid/liquid interface advances past the particle concentrated region ($\emptyset < \emptyset_b$), the pushing of particles by the freezing front can resume and the cycle is repeated until the whole sample is fully frozen.[15] During the freezing of low particle concentration suspensions, the particles may be swept over a large distance before breakthrough can occur, resulting in continuous large pores or dendrites that may evolve into large defects upon sintering.[5,6,8,23] The breakthrough volume fraction ($\emptyset_b$) can be reached over a small advancing distance using highly concentrated slurries, which provides opportunity to achieve green bodies with finer pore sizes. [14,23]

Calculations were conducted to determine the freezing front velocities and the breakthrough volume fraction following the approach of Shanti *et al.*[15] (see the appendix in the supporting information). This analysis indicates that the freezing front velocities were between 0.05 and 0.7 mm/s for freezing in pre-chilled molds at 0ºC and

-80°C respectively. The breakthrough volume fraction is 66.6 vol% solids (1% lower than the maximum packing fraction assumed, 67.6%). Some segregation is expected as the particle concentration in the suspensions was significantly less than the breakthrough volume fraction.

As shown in Figure 9, larger voids/pores were seen with slow freezing (0.13 °C/s; 0°C pre-chilled close-cavity mold) (especially when the solid content of the suspensions was low), while faster freezing (0.5 °C/s; -40°C pre-chilled close-cavity mold) corresponded to smaller voids. In the case where there are large voids, the voids may coalesce and grow larger as the particles between the voids densify during sintering (the regions between the large voids in Figure 9 appear to be reasonably dense). This leads to lower overall density and less overall shrinkage of the sintered compacts. In the absence of large voids (as observed in ZrB_2 specimens freeze cast at -40°C using 54 vol% solid suspension shown in Figure 9(d-f)), the compacts can shrink more during sintering and produce final parts of higher densities.

Large channel-like and dendritic pores are found in the samples produced from aqueous formulations as shown in Figure 6. The lower solids content (45 vol%) and tendency of ice to form large crystals is primarily responsible for this microstructure. No large interconnected channels or dendritic freezing patterns were observed in the sintered samples of ZrB_2 produced with the cyclohexane formulations. Compared to water, cyclohexane tends to solidify in smaller crystal (grain) size resulting in smaller pores in the green body.[21] Some large pores were found in the samples frozen slowly in pre-chilled molds at 0°C (Figure 9 (a-c)) and in the molds filled at ambient temperature particularly from lower solids content suspensions. These large pores appear to form as a combined result of particle rejection at the freezing front and pore coarsening during

sintering. The large pores formed in the freezing stage cannot be eliminated by sintering because they have a large particle coordination number (number of particles surrounding the pore). It is known[30,51-54] that pores with particle coordination number greater than a critical value will tend to grow by merging with the surrounding pores, and thus further densification cannot be achieved.[51,52] In the absence of significantly large channels or pores formed during freezing, samples are more likely to yield higher sintered densities,[23] as shown in Figure 4 because these smaller pores have particle coordination number lower than the critical value.

4.2 Comparison with earlier work in freeze casting, slip casting and dry pressing

Several researchers have reported the successful application of freeze casting to fabricate dense ceramic objects.[14,20-25] A comparison of the present work with the freeze casting systems employed by other researchers is summarised in Table 1. The freeze casting studies presented in Table 1 employed highly concentrated suspensions (with solid content varied from 48 to 60 vol%) in order to maximise the green and sintered densities of the freeze cast compacts. In some cases, when water was used as the solvent, a cryoprotectant was added to disrupt the ice crystal formation, reducing the size of ice crystals and mimimizing the size of pores in the green bodies.[23,25] On the other hand, a cryoprotectant was deemed unnecessary when working with the non-aqueous systems.[14,20-22, 24,]

The removal of large pores likely to exist in the green bodies of many of these investigations is believed to be due to either liquid phase sintering or larger diffusion coefficients of simple oxides relative to ZrB_2. Wildhack and Aldinger[25] used Y_2O_3 for liquid-phase sintering of AlN (due to the formation of Y-Al-O-N liquid phase from the

surface oxide on AlN reacting with the Y_2O_3). This liquid phase formed during sintering is likely to have enabled particle rearrangement, improved removal of large pores and reduced crack formation explaining the high sintered density achieved in their work. Also, many of the ceramics produced by Ceramic Process Systems (CPS)[19-22] contained a liquid phase-sintering aid, such as the silicon nitride and SiAlON compositions or were "easier" to densify oxides such as alumina or zirconia. The alumina freeze cast by Sofie and Dogan[23] reached 98% theoretical density most likely because it was an easy to densify oxide. ZrB_2 is a "difficult-to-densify" ceramic due to its strong covalent bonds, and its low mass diffusion coefficient explaining the lower relative sintered densities in the current work. The work presented in the current paper reports the first time freeze casting has been applied to ZrB_2 to make dense components. The results presented in the previous section, generally agree with the previous known concepts about the influence of freezing temperature (freezing rate) and solid content of the slurries.[3-6,10,14,15,23-25]

As presented in our earlier work, slip cast samples of similar formulation in cyclohexane had green densities 67.3 %TD.[30] When sintered under the same conditions (1 hour dwell at 2100ºC with a heating rate of 5ºC/min), compacts produced using the non-aqueous formulations by slip casting had sintered density 92.4 %TD[30]. The freeze cast specimens in this work had green density similar to the suspension formulation, (~54-59 %TD) but were able to reach 90-91.5 %TD when sintered under the same conditions (1 hour dwell at 2100ºC with a heating rate of 5ºC/min) when pre-chilled molds closed-cavity at -40ºC and below were used. This is slightly surprising given that the green densities of freeze cast ZrB_2 compacts (~54-59 %TD) were much lower than that of slip cast (67.3 %TD).[30] The slip cast bodies green density is higher than those

achieved in freeze casting because of the capillary pressure on the slip cast powder body that occurs when liquid solvent is removed by evaporation. Such capillary consolidation pressure does not exist when the frozen solid solvent is removed from the powder body by sublimation. All the freeze cast ZrB_2 specimens also possessed higher sintered densities (76.2-91.5 %TD) compared to the dry pressed and aqueous slip cast ZrB_2 from our previous work (67.6 and 58.9 %TD green density, respectively)[30] even though the green densities were comparable. This indicates the importance of having a more homogenous (non-aggregated) particle packing to facilitate densification of this material.

4.3 Cracking

Although freeze casting has been employed to produce porous and dense ceramic objects, very little has been reported in the literature about cracking of the objects. In this work, cracking of the freeze cast compacts was found to be prevalent. Macroscopic cracking of the samples tended to occur at the faster freezing rates investigated. These conditions also corresponded to the highest sintered densities and the greatest amount of shrinkage. At the current time we have no definitive explanation of when or how the cracking occurs, but here we discuss two plausible mechanisms, which are currently under investigation.

1. Cracking occurs during freeze drying.

If the surface of the part is dried and then the temperature of the interior increases above the melting temperature of the solvent (at the pressure within the freeze drying chamber), cracking of the interior has been observed to occur.[21,55] Some or all of the

cracking observed in our samples is likely to have been caused by this or a similar mechanism since the temperature of shelves in our freeze dryer where the samples are placed during freeze drying was not controlled (the shelves in our freeze dryer remained at room temperature for all the experiments described in this work).

2. Cracking occurs during sintering.

Elastic stress induced by strain due to differential shrinkage during sintering could cause cracking. The differential shrinkage could occur if there are regions of the green body with large pores that cannot be eliminated during sintering and other regions of the green body have only small pores that are able to be eliminated during sintering. When freeze casting using a pre-chilled close-cavity aluminium mold, the initial freezing rate near the mold surface can be very fast and the freezing rate decreases with distance away from the cooling surface until it reaches steady state with a constant value.[8] Thus, it is possible that the pore size varies with distance from the mold surface as has been reported by other researchers.[7,15,40,46,47] A more homogenous, dense layer of the green body with finer pores is likely to form on the outer surface of the sample and the pore size progressively grows larger with distance from the surface to the centre of the sample. Finer pores are easier to eliminate during sintering and this corresponds to a denser final microstructure and increased shrinkage. Although the solid concentration (i.e. green density) remains the same across the green sample, the central region which consists of clusters of particles separated by larger pores are more difficult to densify and most likely shrink less than the outer surface. The differential shrinkage may cause stresses to be developed during sintering as constraint imposed on the shrinking outer regions by the central region will cause the surface to be in tension and the interior in to be in compression.[56,57] These stresses can only be relieved through the formation of

cracks.[56-58] Although we have a suspicion that differential shrinkage during sintering is playing a role in cracking, cracks caused by the mechanism just described would present as surface cracks rather than internal cracks.

Despite the increased sintered density, faster freezing corresponds to more significant cracking of the freeze cast samples (see Figure 10). This is likely because there is a steeper pore size gradient between the surface and the centre region of the samples and hence, a more significant differential shrinkage with decreasing freezing temperature. Because samples frozen more rapidly tend to possess smaller pores overall, they will likely have greater overall shrinkage resulting in greater differential shrinkage, resulting in more cracking of the samples during sintering.

It appears that a more uniform freezing was achieved by slow freezing in a close-cavity mold pre-chilled to 0^{o}C or open-cavity mold filled at ambient temperature. These samples had either fewer or no visible cracks (Figure 10). In these cases, the final sintered densities were lower than the samples frozen more quickly, due to the presence of large pores. Less overall shrinkage means there is less potential for differential shrinkage and as such, the bodies that do not densify significantly tend not to crack. Currently, slow freezing is suggested as the preferred approach when applying freeze casting to ZrB_2 to create near-net-shaped components. The lower density could be improved by adding some carbon, boron carbide or other sintering aid into the mixture in order to increase the density of the pieces. More research should be conducted to fully understand the mechanisms for the observed macro-cracking of the samples.

5. CONCLUSIONS

Freeze casting can be employed to produce complex-shaped objects from highly concentrated suspensions of ZrB_2. The non-aqueous-based system (cyclohexane) produces objects with higher densities and smaller pores than the aqueous-based system. The influence of two important parameters, the freezing conditions and solid concentration of the non-aqueous-based suspensions, on the final density, microstructure and cracking of freeze cast ZrB_2 has been investigated. The sintered density of the freeze cast compacts was found to increase with increasing freezing rate and with increasing solid concentration in the suspensions. By optimising the freeze casting conditions, relatively high sintered densities can be achieved for ZrB_2; up to 91.5 %TD. Despite the relatively high sintered density, faster freezing was found to cause more significant macroscopic cracking of the samples. Several possible causes for this cracking have been discussed. Parts with fewer or no cracks were obtained in the sintered samples when the suspensions were frozen slowly. However, the sintered density also decreased, as slow freezing resulted in the formation of large pores which were difficult to shrink or remove during sintering.

Acknowledgements

The authors acknowledge the Defence Materials Technology Centre (DMTC) for funding and supporting this work including Silvia's PhD scholarship. Thanks to Roger Curtain at the Advanced Microscopy Facility at the Bio21 Institute of The University of Melbourne who conducted some of the SEM imaging as well as enabling access to Silvia and Carolina for other images. Thanks to Jack Churchill (University Melbourne) for conducting some of the preliminary freeze casting experiments in water. Thanks to Yuko Hayakawa (Tokyo Institute of Technology) for molding the interlocking tiles. Thanks to Yuri Estrin and Andrey Molotnikov (Monash University) for providing the

CAD drawing of the interlocking tile geometry. Thanks to Mitchell L. Sesso for providing lab assistance including bisque firing of samples and for robust feedback and discussions. George V. Franks and Samuel Pinches thank the Australian Research Council for funding Discovery Project DP150102788.

References

1. Franks GV, Tallon C, Studart AR, Sesso ML, Leo S. Colloidal Processing: Enabling Complex Shaped Ceramics with Unique Multiscale Structures. *J. Am. Ceramic Soc.* 2017;100:458-490.

2. Tallon C and Franks GV. Recent Trends in Shape Forming from Colloidal Processing: A Review. *J. Ceramic Soc. Japan*, 2011;119 [3]:147-160.

3. Deville S. Freeze-Casting of Porous Ceramics: A Review of Current Achievements and Issues. *Adv. Eng. Mater.*2008;10:155-169.

4. Fukusawa T, Ando M, Ohji T, Kanzaki S. Synthesis of Porous Ceramics with Complex Pore Structure by Freeze-Dry Processing. *J. Am. Ceram. Soc.*2001;84:230-232.

5. Fukusawa T, Deng ZY, Ando M, Ohji T, Kanzaki S. Synthesis of Porous Silicon Nitride with Unidirectionally Alligned Channels using Freeze-drying Process. *J. Am. Ceram. Soc.* 2002;85:2151-2155.

6. Araki K, Halloran JW. Porous Ceramic Bodies with Interconnected Pore Channels by a Novel Freeze Casting Technique. *J. Am. Ceram. Soc.* 2005;88:1108–1114.

7. Deville S, Saiz E, Nalla RK, Tomsia AP. Freezing as a Path to Build Complex Composites. *Sci.,* 2006;311[5760]:515-518.

8. Deville S, Saiz E, Tomsia AP. Ice-templated Porous Alumina Structures. *Acta Materialia,* 2007;55:1965-1974.

9. Chen RF, Wang CA, Huang Y, M LG, Lin WY. Ceramics with special porous structures fabricated by freeze-gelcasting: Using tert-butyl alcohol as a template. *J. Am. Ceram. Soc.* 2007;90:3478-3484.

10. Tallón C, Moreno R, Nieto IM. Shaping of Porous Alumina Bodies by Freeze Casting. *Adv. Appl. Ceram.* 2009;108:307–313.

11. Zhang Y, Hu L, Han J, Jiang Z. Freeze casting of aqueous alumina slurries with glycerol for porous ceramics. *Ceramics International*. 2010;36:617-621.

12. Landi E, Sciti D, Melandri C, Medri V. Ice Templating of ZrB_2 Porous Architectures. *J. Eur. Ceram. Soc.* 2013;33:1599–1607.

13. Lebreton K, Rodríguez-Parra JM, Moreno R, Nieto IM. Effect of Additives on Porosity of Alumina Materials Obtained by Freeze Casting. *Adv. Appl. Ceram.*2015;114:296–302.

14. Araki K, Halloran JW. New Freeze-casting Technique for Ceramics with Sublimable Vehicles. *J. Am. Ceram. Soc.*2004;87:1859-1863.

15. Shanti NO, Araki K, and Halloran JW. Particle Redistribution during Dendritic Solidification of Particle Suspensions, *J. Am. Ceram. Soc.* 2006;89[8]:2444-2447.

16. How Products are Made, http://www.madehow.com/Volume-6/Popsicle.html, 25, Jan. 2017.

17. Nesbit RA. Formation of Ceramic, etc., Articles. U.S Patent 2,765,512 A; 9th October 1956.

18. Weaver GQ, Nelson BG. Molding Refractory and Metal Shapes by Slip-Casting. U.S Patent 4,341,725 A; 27th July 1982.

19. Novich BE, Lee RR, Franks GV, Ouellette D, Ferber MK. Fabrication of Low Cost and High Performance Ceramic Gas Turbine Engine Components. pp. 111-123 in *Proceedings of the Annual Automotive Technology Development Contractors' Coordination Meeting, Society of Automotive Engineer*, Dearborn, MI, Vol. P-243, 1991.

20. Occhionero MA, Novich BE, Sundback CA. Forming of Complex High Performance Ceramic and Metallic Shapes. US Patent no. 5,047,181, 1991.

21. Sundback CA, Novich BE, Karas AE, Adams RW. Complex Ceramic and Metallic Shaped by Low Pressure Forming and Sublimative Drying. US Patent no. 5,047,182, 1991.

22. Novich BE, Sundback CE, Adams RW. Quickset^{TM} Injection Molding of High Performance Ceramics. in *Ceramic Transactions, Forming Science and Technology for Ceramics*, Vol 26. Edited by M.J. Cima, (Westerville, OH), American Ceramic Society, pp. 157–164, 1992.

23. Sofie SW and Dogan F. Freeze Casting of Aqueous Alumina Slurries with Glycerol. *J. Am. Ceram. Soc.* 2001; 84[7]:1459-1464.

24. Araki K and Halloran JW. Room-Temperature Freeze Casting for Ceramics with Nonaqueous Sublimable Vehicles in the Naphthalene–Camphor Eutectic System. *J. Am. Ceram. Soc.* 2004; 87[11]:2014-2019.

25. Wildhack S and Aldinger F. Freeze Casting of Aluminium Nitride," *Adv. Sci. Technol.* 2006;45:407-412.

26. Lu K. Microstructural Evolution of Nanoparticle Aqueous Colloidal Suspensions during Freeze Casting. *J. Am. Ceram. Soc.* 2007; 90[12]:3753-3758.

27. Lu K and Zhu X. Freeze Casting as a Nanoparticle Material-Forming Method. *Int. J. Appl. Ceram. Technol.* 2008; 5 [3]:219-227.

28. Sundback CA, Franks GV, Lee RR, Novich BE. "Near net shape Fabrication of AGT-5 Ceramic Gas Turbine Rotors using Quickset Injection Molding", *Proceedings of the Annual Automotive Technology Development Contractors' Coordination Meeting*, Society of Automotive Engineers, publication P-256, pp 31-36, 1992

29. Leo S, Tallon C, Franks GV. Aqueous and Nonaqueous Colloidal Processing of Difficult-to-Densify Ceramics: Suspension Rheology and Particle Packing, *J. Am. Ceramic Soc.* 2014; 97 [12]:3897-3817.

30. Leo S, Tallon C, Franks GV. Pressureless Sintering of ZrB_2 Prepared by Colloidal Processing: Particle Packing, Sintering Conditions, and Additives. *J. Am. Ceramic Soc.* 2016; 99 [12]:3883-3892.

31. *CRC Handbook of Chemistry and Physics,* Vol. 79, Edited by D. R. Lide. CRC Press Inc., Boca Raton, Fl, 1998.

32. Wohlfarth Ch. "Supplemet to IV/18"; pp. 377-80 in *Landolt-Börnstein - Group IV Physical Chemistry,* Vol. 25, Edited by M. D. Lechner. Springer-Verlag, Berlin, 2009.

33. Cruickshank AJB and Cutler AJB. Vapor Pressure of Cyclohexane, 25º to 75ºC. *J. Chem. Eng. Data.* 1967;12 [3]:326-329.

34. Stokes RH and Tomlins RP. Thermodynamic Functions of Melting for Cyclohexane. *J. Chem. Thermodyn.* 1974;6 [4]:379-386.

35. Dauber TE and Danner RP. *Data Compilation Tables of Properties of Pure Components,* American Institute of Chemical Engineering, New York, 1985.

36. Rao SP, Tripathy SS, and Raichur AM. Dispersion Studies of Sub-micron Zirconia using Dolapix CE 64, *Colloid Surface A.* 2007;302:553-558.

37. Dakskobler A and Kosmac T. Weakly Flocculated Aqueous Alumina Suspensions Prepared by the Addition of Mg(II) Ions. *J. Am. Ceram. Soc.* 2000;83 [3]:666-668.

38. Tanurdjaja S, Tallon C, Scales PJ, and Franks GV. Influence of Dispersant Size on Rheology of Non-aqueous Ceramic Particle Suspensions. *Adv. Powder Technol.* 2011;22 **[**4]:476-481.

39. Chuanuwatanakul C, Tallon C, Dunstan DE and Franks GV. Controlling the Microstructure of Ceramic Particle Stabilized Foams: Influence of Contact Angle and Particle Aggregation. *Soft Matter*. 2011; 7:11464-11474.

40. Bareggi A, Marie E, Lasalle A and Deville S. Dynamics of the freezing front during solidification of a colloidal alumina aqueous suspension: in situ X-Ray radiography, tomography and modelling, *J. Am. Ceram. Soc.* 2011; 94 [10]:3570-3578.

41. Uhlmann DR, Chalmers B, and Jackson KA. Interaction Between Particles and a Solid-Liquid Interface. *J. Appl. Phys.* 1964; 35 [10]:2986-2993.

42. Körber C, Rau G, Cosman MD, and Cravalho EG. Interaction of Particles and a Moving Ice-liquid Interface, *J. Cryst. Growth.* 1985; 72 [3]:649-662.

43. Rempel AW and Worster MG. Particle Trapping at an Advancing Solidification Front with Interfacial-Curvature Effects. *J. Cryst. Growth.* 2001; 223 [3]:420-432.

44. Peppin SSL, Elliott JAW and Worster MG. Solidification of Colloidal Suspensions. *J. Fluid Mech.* 2006; 554:147-166.

45. Bolling GF and Cissé J. A Theory for the Interaction of Particles with a Solidifying Front. *J. Cryst. Growth.* 1971; 10 [1]:56-66.

46. Waschkies T, Oberacker R, and Hoffmann MJ. Investigation of Structure Formation during Freeze-casting from Very Slow to Very Fast Solidification Velocities. *Acta Materialia,.* 2011; 59 [13]:5135-5145.

47. Koch D, Andresen L, Schmedders T, and Grathwohl G. Evolution of Porosity by Freeze Casting and Sintering of Sol-Gel Derived Ceramics. *J. Sol-Gel Sci. Tech.* 2003; 26 [1-3]:149-152.

48. Li WL, Lu K, and Waltz JY. Freeze Casting of Porous Materials: Review of Critical Factors in Microstructure Evolution. *Int. Mater. Rev.* 2012;57[1]:37-60.

49. Guo JJ and Lewis JA. Aggregation Effects on the Compressive Flow Properties and Drying Behavior of Colloidal Silica Suspensions. *J. Am. Ceram. Soc.* 1999; 82 [9]:2345-2358.

50. Carnahan NF and Starling KE. Equation of State for Nonattracting Rigid Spheres. *J. Chem. Phys.* 1969; 51 [2]:635-636.

51. Dole SL, Prochazka S and Doremus RH. Microstructural Coarsening during Sintering of Boron Carbide. *J. Am. Ceram. Soc.* 1989; 72 [6]:958-966.

52.Shi JL. Relations Between Coarsening and Densification and Mass Transport Path in Solid-state Sintering of Ceramics: Model Analysis. *J. Mater. Res.* 1999:14 [4]:1378-1388.

53. Rahaman MN. *Ceramic Processing,* Ch. 9. CRC Press, Boca Raton, FL, 2007.

54. Castro RR. "Overview of Conventional Sintering"; pp. 1-16 in *Sintering*, Engineering Materials Vol. 35, Edited by R. Castro and K. van Benthem. Springer-Verlag Berlin Heidelberg, 2013.

55. Tian G, Lu Z, Miao K, Zhang H, Li D. Formation of cracks during freeze drying of gelcast ceramic parts. *J. Am. Ceram. Soc.* 2016;98:3338-3345.

56. Lange FF. Processing-Related Fracture Origins: I, Observations in Sintered and Isostatically Hot-Pressed $A1_2O_3/ZrO_2$ Composites. *J. Am. Ceram. Soc.* 1983;66 [6]:396-398.

57. Lange FF and Metcalf M. Processing-Related Fracture Origins: II, Agglomerate Motion and Cracklike Internal Surfaces Caused by Differential Sintering. *J. Am. Ceram. Soc.* 1983; 66 [6]:398-406.

58. Ostertag CP. "Differential Sintering"; pp. 453-9 in *Science of Sintering: New Directions for Materials Processing and Microstructural Control,* Edited by D. P. Uskoković, H. Palmour III, and R. M. Spriggs. Springer-Verlag, US, 1989.

Figures:

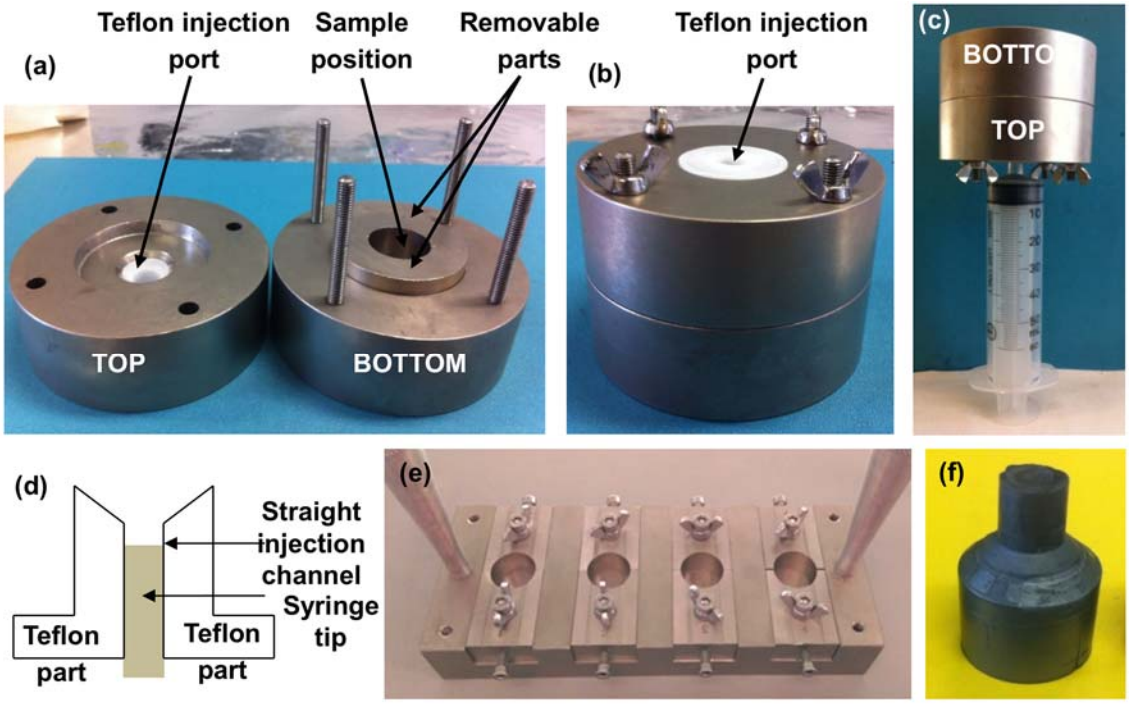

Figure 1. Molds used in this work; Closed-cavity molds (a-d) and open-cavity molds (e). Parts c and d show the filling of the closed-cavity molds with the suspension. (f) Example of cylinder produced using the mold shown in parts a to d.

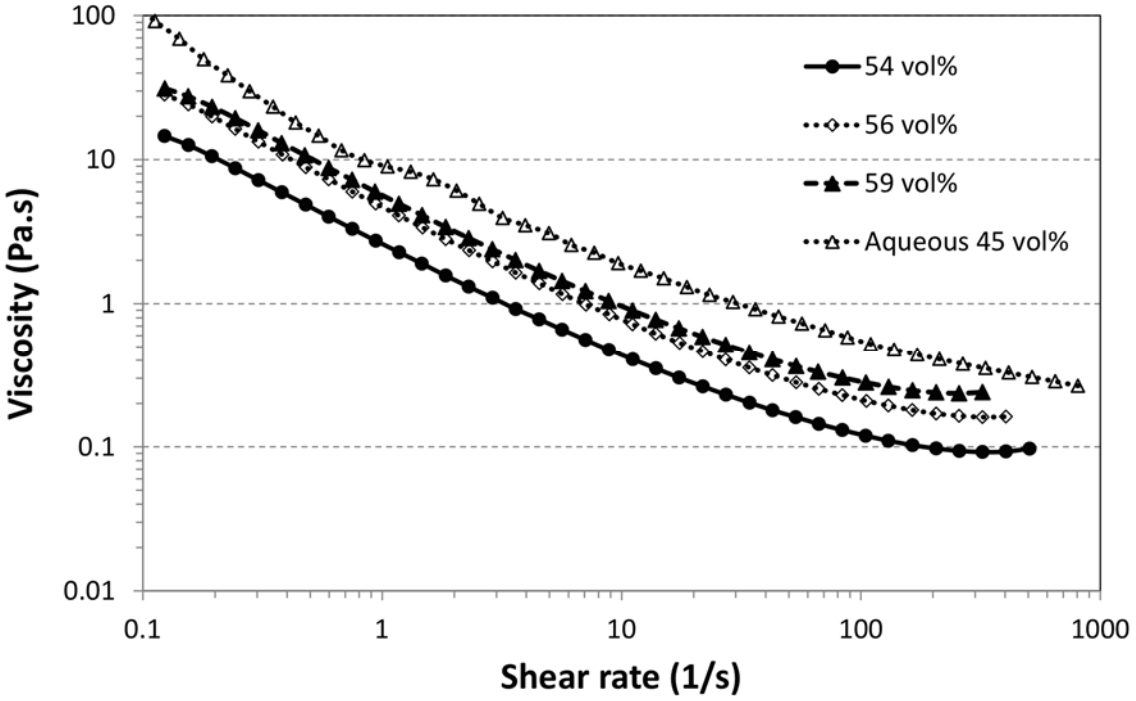

Figure 2. Steady shear viscosity of ZrB_2 with 1.0 wt% Dolapix CE 64 (with respect to powder weight) in water suspensions containing 45 vol% solids compared to ZrB_2 with 1.0 wt% HypermerA70 (with respect to powder weight) in cyclohexane containing 54-59 vol% solids.

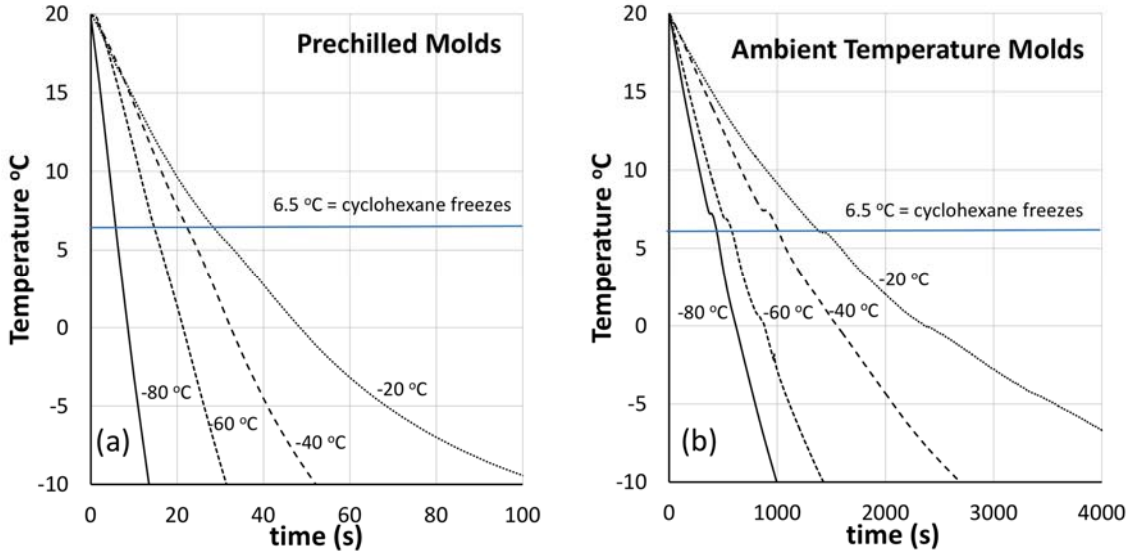

Figure 3. Temperature as a function of time measured with a K-type thermocouple in the center of the cylindrical mold for injection of 55 vol% solids ZrB_2-cyclohexane suspension into (a) pre-chilled closed-cavity molds and (b) ambient open-cavity molds, then placed in freezer set at the temperatures indicated.

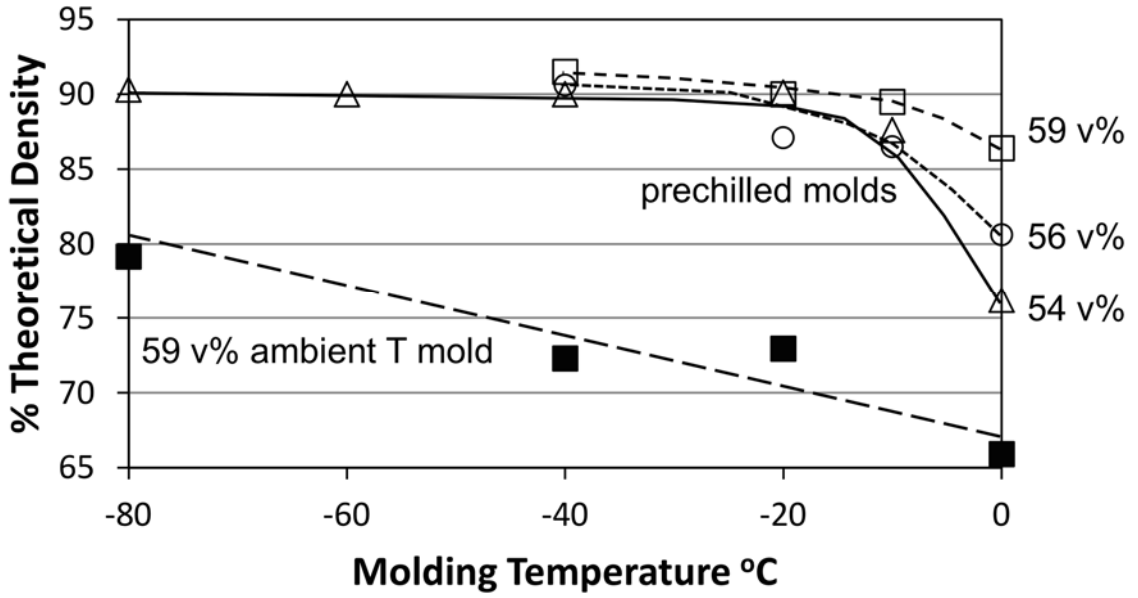

Figure 4. Sintered density of freeze cast ZrB_2 cylinders produced from cyclohexane suspensions at the volume percent solids indicated as a function of the temperature of the freezer for samples injected either into pre-chilled closed-cavity molds or open-cavity ambient temperature molds as indicated. Density indicated as % of theoretical density where full theoretical density of ZrB_2 is 6.1 g/cm^3.

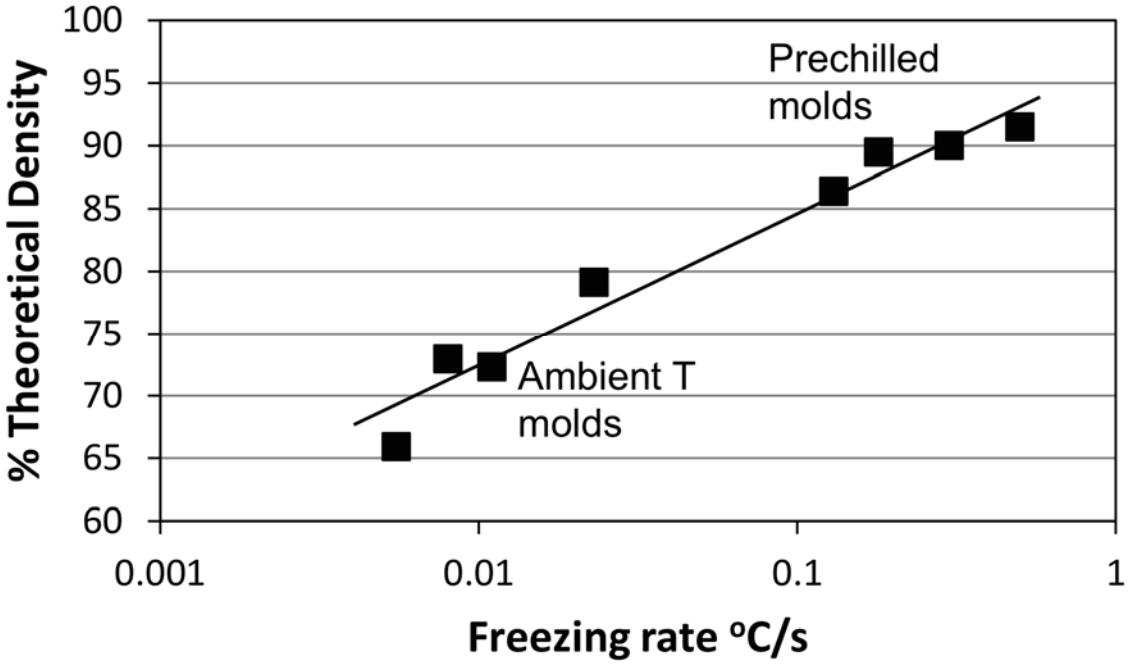

Figure 5. Sintered density of freeze cast ZrB_2 cylinders produced from cyclohexane suspensions at 59 v% solids as a function of freezing rate for samples injected either into pre-chilled molds or ambient temperature molds as indicated. Density indicated as % of theoretical density where full theoretical density of ZrB_2 is 6.1 g/cm^3.

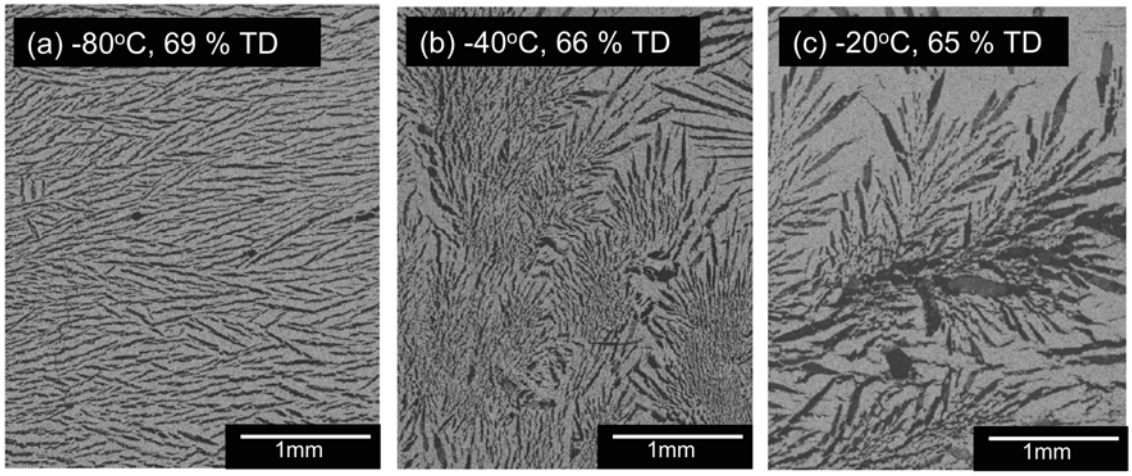

Figure 6. Low magnification SEM images of sintered ZrB_2 produced from 45 vol% solids aqueous suspensions by freezing at (a) -80°C, (b) -40°C and (c) -20°C after injection into an ambient room temperature closed-cavity mold. All samples were sintered in a graphite furnace at 2100°C for 1 hour.

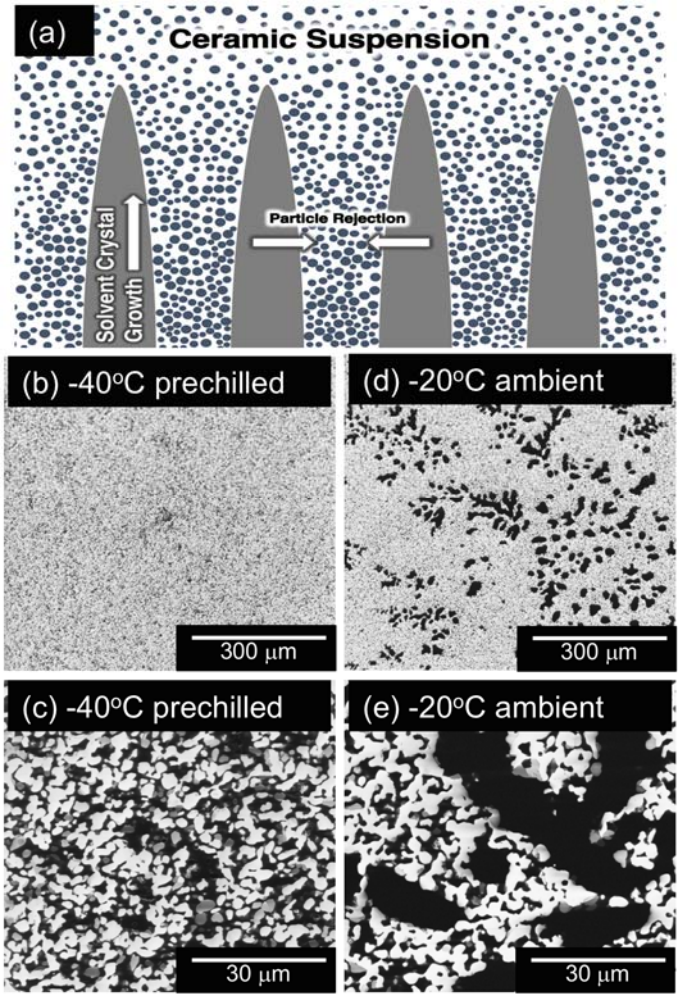

Figure 7. (a) Schematic illustration of how solvent crystals can push particles ahead of the solidification front as they slowly grow during freezing of the solvent. Adapted from Deville, reference 3. (b) Macrostructure and (c) microstructure of green body after bisque firing at 1600ºC for 30 mins in argon for 54 vol% solids cyclohexane suspension freeze cast by injection into a -40ºC prechilled mold. No pores greater than about 10 to 20 microns are observed. (d) Macrostructure and (e) microstructure of green body after bisque firing at 1600ºC for 30 mins in argon for 54 vol% solids cyclohexane suspension freeze cast by placing a mold filled at ambient temperature into a -20ºC freezer. Many dendritic pores are observed with dendrite width about 20 microns and lengths up to 100 or more microns.

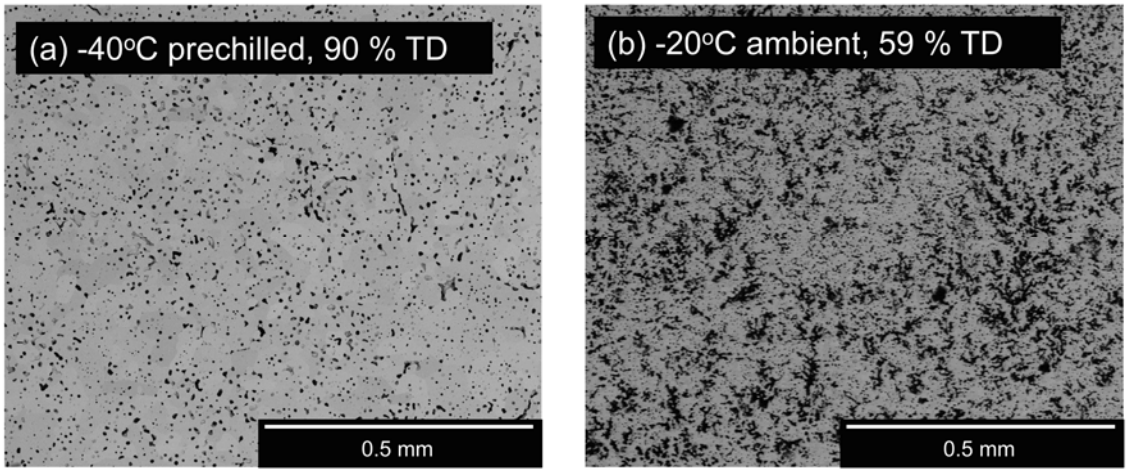

Figure 8. Low magnification SEM images of sintered ZrB_2 produced from 54 vol% solids cyclohexane suspensions by at (a) injection into a -40°C pre-chilled closed-cavity mold and (b) freezing at -20°C after filling the mold at ambient temperature. Both samples were sintered in a graphite furnace at 2100°C for 1 hour.

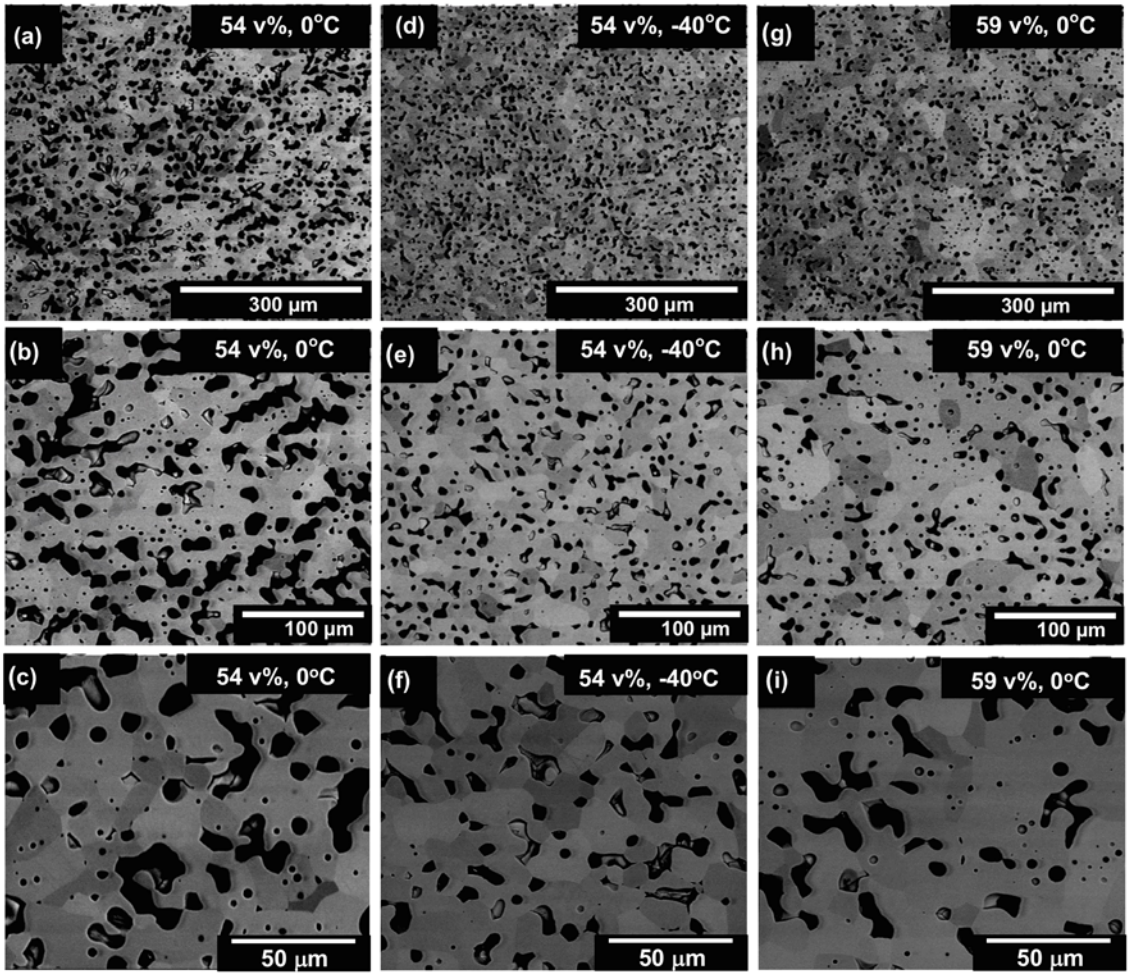

Figure 9. SEM micrographs of sintered ZrB_2 samples freeze cast in pre-chilled closed-cavity molds at three different magnifications. (a -c) Freeze cast using 54 vol% solids suspension at freezing temperature of 0°C (sintered density of 76.2 %TD). (d-f) Freeze cast using 54 vol% solids suspension at freezing temperature of -40°C (sintered density of 90.0 %TD). (g-j). Freeze cast using 59 vol% solid at freezing temperature of 0°C (sintered density of 88.5 %TD). The samples were sintered in a graphite furnace at 2100°C for 1 hour.

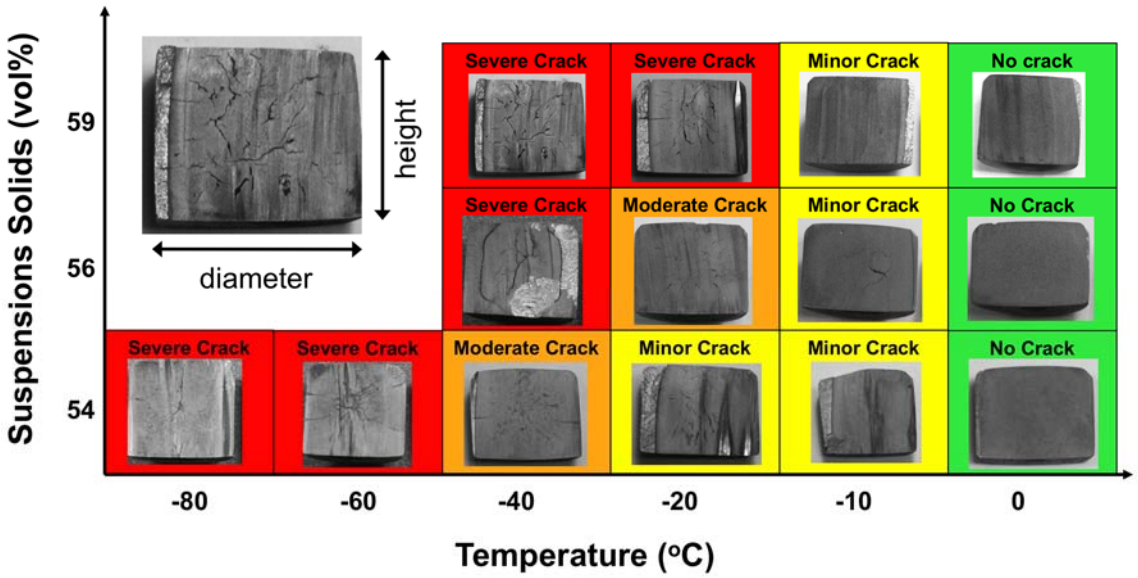

Figure 10. Photographs of cross sections of cylinders produced by freeze casting cyclohexane suspensions with the solids concentration indicated on the y-axis into pre-chilled close-cavity molds at the temperatures indicated on the x-axis.

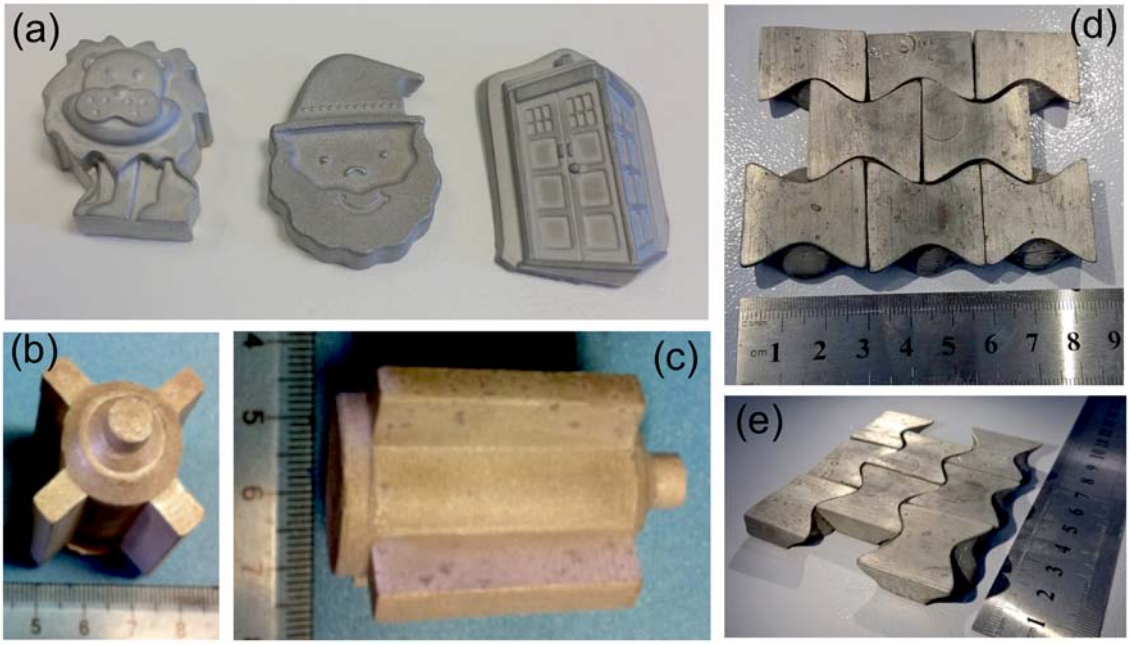

Figure 11. Complex-shaped ZrB_2 components produced by freeze casting. a) Novelty objects produced from soft rubber open-cavity molds filled at ambient temperature and frozen at -40ºC. b) and c) The rotor-shaped objects were freeze cast in an aluminium close cavity mold pre-chilled to 0ºC using suspensions containing 59 vol% solids. d) and e) Interlocking tiles molded in an aluminium open-cavity mold filled at ambient temperature with suspensions containing 59 vol% solids and frozen at -40ºC. After firing at 2100ºC in the Red Devil furnace, the parts had densities varying form 65% to 80% theoretical density.

Table 1. Summary of characteristics of freeze cast objects in the current work and those reported in the literature.

Material	Solids content	Solvent	Sample dimensions*	Freezing conditions	Sintering conditions	Sintered density (%TD)	Ref
ZrB_2 (D_{50} = 2.3 µm)	54-59 vol% solid suspension	cyclohexane	Cylindrical D = 20 mm H = 16.6 mm	Aluminium mold Pre-chilled or ambient filling, 0 to -80°C	2100°C, 1 hour dwell, 5°C/min	76-91.5 pre-chilled mold 65- 80 ambient filled mold	Current paper
ZrB_2 (D_{50} = 2.3 µm)	45 vol% solid suspension	water	Cylindrical D = 20 mm H = 16.6 mm	Aluminium mold Pre-chilled or ambient filling, 0 to -80°C	2100°C, 1 hour dwell, 5°C/min	64-70 pre-chilled or ambient filled molds	Current paper
Al_2O_3 (D_{50} = 0.4 µm)	50.8 vol% solid suspension	camphene ($T_{melting}$ = 44-48°C)	Cylindrical D = 10 mm H = 5 mm	Polyurethane mold from 55°C to room temperature	1600°C, 4 hours dwell, 5°C/min	98.4	14
Al_2O_3 (D_{50} = 0.4 µm)	48 vol% solid suspension	40 wt% Naphthalene – 60 wt% Camphor	Cylindrical D = 10 mm H = 5 mm	Polyurethane mold from 55°C to room temperature	1600°C, 4 hours dwell, 5°C/min	99.5	24
Al_2O_3 (D_{50} = 0.37 µm)	60 vol% solid suspension	water - Cryoprotectant: glycerol	Cylindrical D = 25 mm H = 12.5 mm	Silicone mold from room temperature to -35°C	1650°C, 5 hours dwell, 5°C/min	98	23
AlN (70% D_{50} (coarse) = 8.1 µm, 30% D_{50} (fine) = 1.5 µm) with 2 wt% Y_2O_3	55 vol% solid suspension	water - Cryoprotectant: glycerol	Rectangular L = 12 mm W = 12 mm H = 50 mm	Pre-chilled metal mold -40°C	1900°C, 1 hour dwell	98	25
SiAlON (D_{50} = 0.5 µm) cyclohexane	55 vol% solid suspension	cyclohexane	Ring ID = 19.6 mm OD = 40.91 mm	Pre-chilled steel mold -78°C	Not reported	96	20-22

* D = diameter, ID = inner diameter, OD = outer diameter, H= height, L = length, and W = width

Supporting Information: Freeze Casting for Near-Net-Shaping of Dense Zirconium Diboride Ceramics, Silvia Leo, Laura Jukes, Samuel Pinches, Carolina Tallon, George V. Franks

Table S1. Freezing rate between 10 and 7°C measured in centre of cylinder mold for both pre-chilled and ambient filled molds.

Mold Temperature °C	Pre-chilled Mold Freezing Rate °C/s	Ambient Mold Freezing Rate °C/s
-80	2.5	0.023
-60	1.0	0.023
-40	0.5	0.011
-20	0.3	0.008
-10*	0.18	0.007
0*	0.13	0.0055

* Extrapolated from measurement at colder temperatures

Table S2. Sintered densities (% of theoretical density) of cylinders freeze cast from 45 vol% aqueous suspensions.

	-80°C	-40 °C	-20 °C
Pre-chilled injection	64.2 %TD	68.3 %TD	70.0 %TD
Ambient fill then freeze	68.7 %TD	65.9 %TD	64.8 %TD

Table S3. Sintered densities (% of theoretical density) of ZrB_2 (a) (pre-chilled injections) and (b) ambient filled ice cube tray freezing) as a function of freezing temperature for specimens freeze cast using suspensions containing 54-59 vol% solid.

temperature	-80 °C	-60 °C	-40 °C	-20 °C	-10 °C	0 °C
(a) Pre-chilled mold						
59 vol%			91.5%	90.0%	89.5%	86.4%
56 vol%			90.6%	87.1%	86.5%	80.6%
54 vol%	90.3%	90.0%	90.0%	90.1%	87.6%	76.2%
(b) Ambient fill then freeze – 59 vol%	79.2%		72.3%	73.0%		65.9%

Appendix: Calculation of the freezing front velocities and the breakthrough volume fractions of ZrB_2 suspensions.

(1) Freezing front velocities

The freezing time (t_f) can be estimated using the following Planck's equation:[A1]

$$t_f = \frac{\Delta H.\rho}{(T_f - T_a)}\left[\frac{PD}{h} + \frac{RD^2}{\lambda_{susp}}\right] \qquad \text{(in secs)} \qquad \textit{Eq. (A1)}$$

where ΔH is the latent heat of fusion (31.69 kJ/kg for cyclohexane)[A2], ρ is the density of the freezing material (779 kg/m^3 for cyclohexane), T_f is the freezing temperature of the material (6.5°C)[A3], T_a is the freezer temperature, P and R are shape constants (0.25 and 0.0625, respectively, for infinite cylinder)[A4], h is the heat transfer coefficient of the cold surface (4003 W/m^{2}K)[A5], D is the thickness or diameter of the specimen (0.02 m), and λ_{susp} is the thermal conductivity of the suspension. The thermal conductivity of the suspension is given by the following relation:[A6]

$$\lambda_{susp} = \lambda_1\left[1 + 3\phi_2\beta + 3{\phi_2}^2\beta^2\left(1 + \frac{\beta}{4}\right)\right] \qquad \textit{Eq. (A2)}$$

and

$$\beta = \frac{\lambda_2 - \lambda_1}{\lambda_2 + 2\lambda_1} \qquad \textit{Eq. (A3)}$$

where λ_1 and λ_2 are the thermal conductivity of the solvent (0.13 W/mK)[A7] and the particles (85 W/mK for ZrB_2)[A8] , ϕ_2 is the volumetric concentration of the particles.

In this calculation, freezing is assumed to initiate at the outer diameter of the cylindrical sample and towards the centre of the sample. Thus, the freezing velocity ($\upsilon_{freezing}$) can be estimated by the following equation:

$$\upsilon_{freezing} = \frac{(D/2)}{t_f} = \frac{10}{t_f} \qquad \text{(in mm/s)} \qquad \textit{Eq. (A4)}$$

The results of these calculations are presented in **Table A1**. It can be seen that the freezing speed increases with decreasing freezing temperature and with increasing solid concentration in the suspensions.

Table A1. Thermal conductivities of the suspensions, freezing times and freezing velocities calculated for different solid concentrations in the suspensions and different freezing temperatures.

ϕ_2	λ_{susp} (W/mK)	Ta (°C)	t_f (secs)	t_f (mins)	$\upsilon_{freezing}$ (mm/s)
0.54	0.4804	0	202.40	3.373	0.049
0.54	0.4804	-20	49.65	0.827	0.201
0.54	0.4804	-40	28.29	0.472	0.353
0.54	0.4804	-60	19.78	0.330	0.505
0.54	0.4804	-80	15.21	0.253	0.657
0.56	0.4987	0	195.12	3.252	0.051
0.56	0.4987	-20	47.86	0.798	0.209
0.56	0.4987	-40	27.27	0.455	0.367
0.56	0.4987	-60	19.07	0.318	0.524
0.56	0.4987	-80	14.66	0.244	0.682
0.59	0.5270	0	184.90	3.082	0.054
0.59	0.5270	-20	45.35	0.756	0.220
0.59	0.5270	-40	25.85	0.431	0.387
0.59	0.5270	-60	18.07	0.301	0.553
0.59	0.5270	-80	13.89	0.232	0.720

(2)Breakthrough volume fraction

The equation to estimate the breakthrough volume fraction (ϕ_b) of the suspension during freezing is given by Shanti *et al.*:[A9]

$$\phi_b = \phi_m - W \qquad \textit{Eq. (A5)}$$

$$W = \left(\frac{kT}{4\pi a^2 \gamma}\right)^{1/3} \qquad \textit{Eq. (A6)}$$

where ϕ_m is the volume fraction of particles at maximum packing (the maximum packing densities achieved by slip casting was used as approximations for ϕ_m; ϕ_m = 0.676), k is the Boltzmann's constant (1.38 x 10^{-23} m^2kg/s^2K), T is the freezing temperature, a is the radius of the particles (1.15 x 10^{-6}), γ is the surface tension of the solvent at its freezing point (0.02685 J/m^2)[A10].

Table A2. The values of breakthrough volume fraction of ZrB_2 suspensions as a function of freezing temperature.

T		***W***	$\boldsymbol{\phi_b}$
(in °C)	**(in K)**	**ZrB_2**	**ZrB_2**
0	273	0.00203	0.6738
-20	253	0.00199	0.6739
-40	233	0.00193	0.6739
-60	213	0.00187	0.6740
-80	193	0.00181	0.6741

Based on this calculation, the freezing temperature (T) did not affect ϕ_b significantly.

Appendix references

[A1] R. Planck, *Beitrage zur Berechnung und Bewertung der Gefriergeschwindigkeit von lebensmitteln*. Beih. Z. Ges. Kalteind., Reihe 3, H. 10. Berlin, VDI-Verlag, 1941.

[A2] B. E. Poling, G. H. Thomson, D. G. Friend, R. L. Rowley, and W. V. Wilding, "Physical and Chemical Data"; pp. 150-187 in *Perry's Chemical Engineers' Handbook,* 8th ed., Edited by D. W. Green. McGraw-Hill, New York, 2008.

[A3] *CRC Handbook of Chemistry and Physics,* Vol. 79, Edited by D. R. Lide. CRC Press Inc., Boca Raton, Fl, 1998.

[A4] Q. T. Pham, "Extension to Planck's Equation for Predicting Freezing Times of Foodstuffs of Simple Shapes," *Int. J. Refrig.*, **7** [6] 377-83 (1984).

[A5] R. Asthana, A. Kumar, and N. B. Dahotre, *Materials Processing and Manufacturing Science,* Ch. 2. Elsevier, Burlington, MA, 2006.

[A6] A. De Marcos, B. Naït-Ali, N. Tessier-Doyen, A. Alzina, C. Pagnoux, and C. S. Peyratout, "Influence of the Ice Front Velocity and of the Composition of Suspensions on Thermal Properties of Bentonite Materials Prepared using Freeze–Casting Process," *J. Eur. Ceram. Soc.*, **34** [16] 4433-41 (2014).

[A7] T. E. Daubert, R. P. Danner, H. M. Sibul, and C. C. Stebbins, *Physical and Thermodynamic Properties of Pure Compounds: Data Compilation*, extant 1994 (core with 4 supplements), Taylor & Francis, Bristol, PA.

[A8] J. W. Zimmermann, G. E. Hilmas, W. G. Fahrenholtz, R. B. Dinwiddie, W. D. Porter, and H. Wang, "Thermophysical Properties of ZrB_2 and ZrB_2–SiC Ceramics," *J. Am. Ceram. Soc.,* **91** [5] 1405-11 (2008).

[A9] N. O. Shanti, K. Araki, and J. W. Halloran, "Particle Redistribution during Dendritic Solidification of Particle Suspensions," *J. Am. Ceram. Soc.,* **89** [8] 2444-2447 (2006). Same as Ref 15 in the main text.

[A10] J. A. Dean, *Lange's Handbook of Chemistry,* 15th ed., Section 5. McGraw-Hill, New York, 1999.